Computers & Fluids 88 (2013) 298–312

Contents lists available at ScienceDirect

Computers & Fluids

journal homepage: www.elsevier.com/locate/compfluid

Multi-objective aerodynamic shape optimization using MOGA coupled to advanced adaptive mesh refinement

Mohammad Kouhi [a,b,*], Dong Seop Lee [a,1], Gabriel Bugeda [a,b,1,2], Eugenio Oñate [a,b,1,2]

[a] International Center for Numerical Methods in Engineering (CIMNE), Edificio C1, Gran Capitan, 08034 Barcelona, Spain
[b] Universitat Politècnica de Catalunya (UPC), Gran Capitan, 08034 Barcelona, Spain

ARTICLE INFO

Article history:
Received 7 February 2012
Received in revised form 30 July 2013
Accepted 30 August 2013
Available online 15 September 2013

Keywords:
Reconstruction/multi-objective optimization
Shape optimization
Adaptive remeshing
Euler equation
MOGA

ABSTRACT

This paper demonstrates the big influence of the control of the mesh quality in the final solution of aerodynamic shape optimization problems. It aims to study the trade-off between the mesh refinement during the optimization process and the improvement of the optimized solution. This subject is investigated in the transonic airfoil design optimization using an Adaptive Mesh Refinement (AMR) technique coupled to Multi-Objective Genetic Algorithm (MOGA) and an Euler aerodynamic analysis tool. The methodology is implemented to solve three practical design problems; the first test case considers a reconstruction design optimization that minimizes the pressure error between a predefined pressure curve and candidate pressure distribution. The second test considers the total drag minimization by designing airfoil shape operating at transonic speeds. For the final test case, a multi-objective design optimization is conducted to maximize both the lift to drag ratio (L/D) and lift coefficient (Cl). The solutions obtained with and without adaptive mesh refinement are compared in terms of solution improvement and computational cost. Numerical results clearly show that the use of adaptive mesh refinement can improve the solution accuracy while reducing significant computational cost in both single- and multi-objective design optimizations.

1. Introduction

Aerodynamic shape optimization is one of the most important engineering problems which has got a lot of interest due to the large number of requests from the aircraft companies. Many investigations have been carried out over the past two decades in order to speed up the optimization process and improve the optimality of the optimized design. Two main numerical optimization methodologies are studied massively by the researchers in the field of aerodynamic shape optimization; gradient-based methods and Genetic Algorithms (GAs).

Gradient-based methods rely on sensitivities (gradients) of the objective function respect to the design parameters. Sensitivities are considered as the direction for updating design parameters. Firstly, the traditional finite difference was implemented for evaluating sensitivities in aerodynamic shape optimization problems [1,2]. This method suffers from the fact that the computational cost is proportional to the number of design variables. The control theory resolved this drawback via presenting a family of sensitivity derivation methodologies called adjoint method. Using the adjoint method, the cost of sensitivity computation is virtually independent of the number of design variables. As the first attempt, Pironneau [3] applied the control theory for the shape optimization. Jameson and his group [4–6] derived the adjoint method formulation for inviscid/viscous compressible flows with shock waves. Although the continuous adjoint method is studied in [7,8], the discrete adjoint method has gained more popularity recently, due to its straightforward formulation and its ability to easily treat the boundary conditions in viscous problems ([9,10]). Even though gradient-based methods require much less objective function evaluations, they suffer from some unfavorable requirements such as smoothness of the design space, an appropriate initial guess and existence of only one single global optimum [11,12]. Indeed, for handling multi-objective optimization problems, it is necessary to define a global objective function by making a linear combination of the available objective functions through different weights [6,13]. This method is strongly sensitive to the assumed weight coefficients in a way that some optimal solutions may be lost if inappropriate weights are selected. Moreover, multiple optimization runs are required to be performed in order to compute Pareto fronts.

For these reasons, researchers motivated to implement GAs which are based on the process of natural selection instead of

* Corresponding author at: International Center for Numerical Methods in Engineering (CIMNE), Edificio C1, Gran Capitan, 08034, Barcelona, Spain. Tel.: +34 932057016/934016200; fax: +34 934016517/934016894.
E-mail addresses: kouhi@cimne.upc.edu (M. Kouhi), ds.chris.lee@gmail.com (D.S. Lee), bugeda@cimne.upc.edu (G. Bugeda), onate@cimne.upc.edu (E. Oñate).
[1] Tel.: +34 932057016; fax: +34 934016517.
[2] Tel.: +34 934016200; fax: +34 934016894.

0045-7930/$ - see front matter © 2013 Elsevier Ltd. All rights reserved.
http://dx.doi.org/10.1016/j.compfluid.2013.08.015

sensitivities having the capability to escape from local optima toward finding the global solution [14,15]. On the other hand, GAs are able to generate Pareto fronts in a single optimization run by improving the objective functions simultaneously and independently [15]. Firstly, GAs was studied by Gage and Kroo [16] and Crispin [17] for aerodynamic shape optimization problems. Quagliarella and Cioppa [18] applied GAs to find shockless airfoils while Crossley and Laananen [19] used them for helicopter design. Periaux et al. [20] demonstrated the efficiency of GAs to deal with complex aerodynamic optimization problems using parallel computers. Based on the concept of multi-layered hierarchical topology, Wang et al. [21] studied the parallel hierarchical genetic algorithms for a multiple element airfoil. Furthermore, GAs are implemented to multi-component airfoil design [22], inverse design of wings [23] and many other occasions of the aerodynamic shape optimization [24–29]. A large number of investigations have been carried out in the field of multidisciplinary design of aeronautical systems using GAs due to the unique ability of GAs in handling multi-objective optimization problems [30–32]. The main problem of the GAs approach is the computational expense as they require many generations in order to find the global optima. Approximate models [33], hybrid methods [34,35] and parallel algorithms [20,21] successfully have cured this difficulty.

It is clear that the only common issue in the both aerodynamic shape optimization approaches, gradient-based methods and GAs, is the numerical solution of flow equations using CFD codes for evaluating the objective function. Many investigations have been performed over the past two decades in order to improve the accuracy of the CFD simulations while speeding them up. A part of these investigations led to the development of the so called adaptive mesh refinement (AMR) technique in the CFD field. The basic idea behind the adaptive mesh refinement is the control of the mesh resolution by generating an enough fine mesh near the zones where the solution error is high and assigning a coarse mesh to the rest of the domain. AMR schemes are able to improve the accuracy of the flow solution around the high-error zones such as boundary layers, stagnation points and shock waves. Furthermore, AMR techniques can be considered as a capable tool for reducing the computational cost of the flow simulation since they let the analyzer avoid using a fine mesh in all over the domain.

Two main components of adaptive refinement methods are a reliable error estimator/indicator and a mesh refinement strategy. In compressible flow problems, two main categories of error indicators are developed by the researchers. The first one is based on the gradient of a flow variable such as Mach number or density inside the element [36] while in the second category the error indicator is approximated by a derivative one order higher than interpolation functions [37,38]. In order to get a mesh with an equi-distribution of error inside the domain, a mesh refinement strategy must be implemented to generate the new adapted mesh using the information obtained from the error indicator. Mesh refinement is performed through several different methodologies such as *R*-method [39,40], *H*/*P*-method [41,42] and *M*-method [43,37].

Although the efficiency of AMR tools for aerodynamic analysis problems in providing accurate CFD results is now fairly well established [36–38,41,43,42], no work has studied the effect of AMR in aerodynamic shape optimization problems (in terms of computational cost and solution improvement). However, a few researches have been carried out using AMR for each design candidate of the optimization [44,45,35] but they do not show the efficiency of the adaptive mesh in comparison with the uniform one. In this category, the works done by Bugeda and Oñate [44,45] can be mentioned where they have developed a methodology which utilizes adaptive mesh for each design in a suitable manner. Their methodology is based on the derivation of the sensitivity of the nodal coordinates and some flow variables with respect to the design variables to project the remeshing parameters from the old design to the new one.

The main objective of this paper is to show the trade-off between the AMR during the optimization process and the quality of the optimized solution in terms of the improvement and the computational cost. On the other hand, this work demonstrates the capability of AMR in giving better optimization results using less computational cost. Different test cases have been used to compare the behavior of the optimization process with and without the use of AMR strategies. The selected test cases for these comparisons are intentionally simple as the objective of this study is not to show the actual capabilities of the state of the art strategies for the optimization of realistic configurations. The inviscid flow field equations (Euler) and simple geometries have been used for the achievement of the objectives set in the research. The use of more complex test cases involving arbitrary geometries and more advanced fluid flow equations (taking into account viscous and turbulent phenomena) would have prevented the simple interpretation of results when trying to discriminate the effect of AMR strategies from the rest of phenomena involved in the analyses. In any case, the influence of the AMR strategies in the solution of the presented test cases can be easily extrapolated to more complex problems.

In this paper, two optimization methods are considered; the first method uses the Multi-Objective GA (MOGA) [46,47] associated with adaptive mesh refinement technique while the second method uses the MOGA coupled with a conventional mesh technique (uniform mesh). Both methods utilize an Euler flow analyzer [48] and they are implemented to three practical CFD design problems. The first test case considers the reconstruction of transonic airfoil design optimization. For the second test, one of important aerodynamic challenges; airfoil design optimization for drag minimization subject to geometry constraint is considered. For the final design test case a multi-objective transonic airfoil design optimization with two constraints on geometry and aerodynamic performance is conducted. In the first test case, both the MOGA with adaptive and uniform mesh methods are validated by minimizing the pressure error between a predefined pressure and candidate pressure distribution over an airfoil/wing operating at transonic flight conditions. Through these single- and multi-objective test cases, the optimization performances of both MOGA with adaptive and uniform mesh techniques are compared in terms of solution quality and computational cost.

Numerical results obtained from the single- and multi-objective design optimizations show the direct benefits of adaptive remeshing in the reduction of the total computational cost. Indeed, it is observed that the best improvement of the optimal solution using less computational cost is obtained when an adaptive remeshing technique is coupled with the optimum design strategy. The paper will demonstrate how to reduce computational cost and how to improve solution optimality using adaptive remeshing techniques coupled to MOGA for solving complex design problems. It is to clarify that the convergence rate is the matter of optimization strategy and is not to be changed by using different mesh qualities. For this reason, this paper does not aim to compare the convergence rate of presented test cases.

The test cases presented in this paper have been selected taking into account their simplicity in order to allow for clear conclusions from their results. Clearly, they are rather academic test cases, but the intention of the authors has never been to show the state of the art capabilities of available optimization techniques. The complexity of more realistic test cases could mask the benefits of integrating AMR techniques in the optimization process.

The rest of paper is organized as follows; Section 2 describes the adaptive mesh refinement technique and MOGA. Section 3

explains the aerodynamic analysis tool named PUMI and its validation. Section 4 conducts three real-world aerodynamic design optimizations. Section 5 concludes overall numerical results and future research avenues.

2. Methodology

2.1. Multi-Objective Genetic Algorithms (MOGAs)

For the MOGA, in-house software named Robust Multi-objective Optimization Platform (RMOP) is utilized. It is a distributed/parallel computational intelligence framework which is a collection of population based algorithms including Genetic Algorithm (GA) [14,15] and Particle Swarm Optimization (PSO) as shown in Fig. 1. In this paper, a GA searching method in RMOP is used and it is denoted as MOGA. MOGA uses a Pareto tournament selection operator which ensures that the new individual is not dominated by any other solutions in the tournament. RMOP is easily coupled to any analysis tools such as CFD, Finite Element Analysis (FEA) and/or Computer Aided Design (CAD) systems. Details of RMOP and its engineering design applications can be found in Refs. [46,47].

In this paper, MOGA is coupled with both a conventional mesh technique and the advanced adaptive mesh refinement strategy described in Section 2.2. In this research, the design variables are encoded based on real numbers. The tournament selection without replacement is selected here since it is efficient in programming. A simple single-point crossover operator is utilized with an 80% probability of combination, as the use of smaller values was observed to deteriorate the GA performance. After the crossover, non-uniform mutation is performed while the mutation probability is set to 10%. Each generation consists of 20 individuals and the termination criterion is predefined by the number of generation. In all the test cases, the initial population is created randomly. For the constraint handling, the linear penalty method is used in such a way that a weighted sum of the individual constraint violation is added to its fitness value if the constraint is not satisfied.

2.2. Adaptive remeshing strategy

This paper utilizes the error indicator E introduced by Löhner [49] which is a combination of gradient based and curvature based error indicators coupling with the H-method as the refinement strategy. This error indicator can be defined as Eq. (1)

$$(E^{old})^i_{kl} = \frac{(D^2)^i_{kl}}{(D^1)^i_{kl} + (D^0)^i_{kl}} \quad \text{for } k,l = 1,2,3 \tag{1}$$

where $(E^{old})^i$ is the error corresponding to ith node and D^0, D^1 and D^2 are representations of mean, 1st-order derivative and 2nd-order derivative of the flow variable in general multidimensional forms which can be defined as

$$\begin{aligned}(D^0)^i_{kl} &= h^2 c_n \int_\Omega |N^i_{,k}|\,|N^j_{,l}|\,|U_j| d\Omega \\ (D^1)^i_{kl} &= h^2 \int_\Omega |N^i_{,k}|\,|N^j_{,l} U_j|\, d\Omega \\ (D^2)^i_{kl} &= h^2 \Big| \int_\Omega N^i_{,k} N^j_{,l} U_j\, d\Omega \Big|\end{aligned} \tag{2}$$

where the $(.)_{,k}$ and $(.)_{,l}$ denote the first-order derivative with respect to kth and lth directions, respectively, corresponding to x, y and z directions. c_n is a constant depending on the discretization technique, N^j and U_j are the shape function and the flow variable, respectively, corresponding to jth node. Therefore, the error matrix E is obtained as

$$E^{old} = \begin{bmatrix} E^{old}_{xx} & E^{old}_{xy} & E^{old}_{xz} \\ E^{old}_{yx} & E^{old}_{yy} & E^{old}_{yz} \\ E^{old}_{zx} & E^{old}_{zy} & E^{old}_{zz} \end{bmatrix} \tag{3}$$

It is assumed that the new element size h^{new} is proportional to old element size h^{old} by a factor called ξ which is defined as

$$\xi = \frac{h^{new}}{h^{old}} \tag{4}$$

The improved error related to the new mesh has the form shown in Eq. (5)

$$(E^{new})^i_{kl} = \frac{\xi^2 \left(D^2\right)^i_{kl}}{\xi \left(D^1\right)^i_{kl} + \left(D^0\right)^i_{kl}} \tag{5}$$

Given the desired error indicator value E^{new} for the improved mesh, the reduction factor ξ is given by

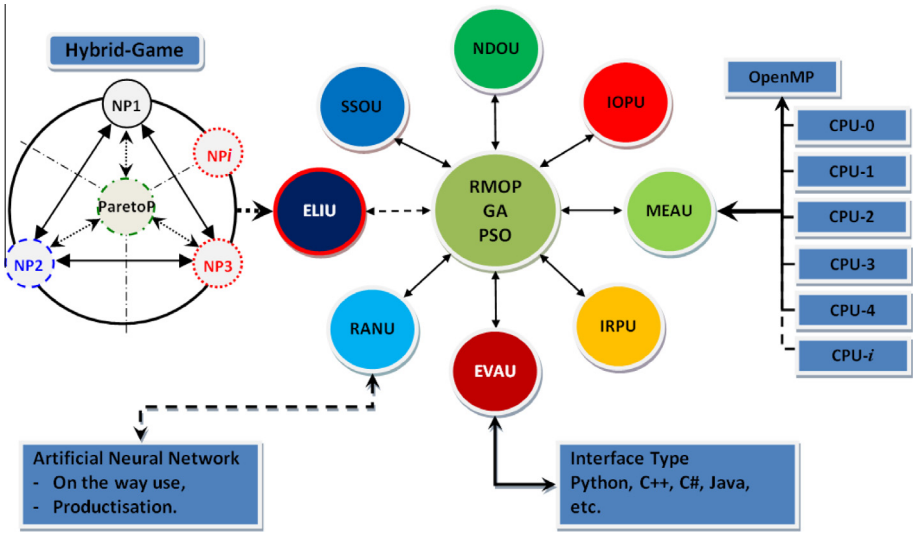

Fig. 1. Topology of robust multi-objective optimization platform.

$$\xi_{kl}^{i}=\frac{E^{new}}{(E^{old})_{kl}^{i}}\frac{(D^{1})_{kl}^{i}+\sqrt{\left[(D^{1})_{kl}^{i}\right]^{2}+4(D^{0})_{kl}^{i}\frac{(E^{old})_{kl}^{i}}{E^{new}}\left[(D^{1})_{kl}^{i}+(D^{0})_{kl}^{i}\right]}}{2[(D^{1})_{kl}^{i}+(D^{0})_{kl}^{i}]} \quad (6)$$

In 2D case, once ξ_{xx} and ξ_{yy} are obtained for each element, the minimum of these two values is replaced in Eq. (6) to calculate the new element size. It is worth noting that in the current methodology only a new element size is prescribed for each element and stretching is not considered. This value is assigned to the corresponding element in the background mesh to generate a new one. By predefining the minimum and maximum element sizes, the computed element size is checked to be in this desirable range. If this condition is not satisfied, the minimum or maximum element size is considered.

Based on the *H*-method for refinement strategy, an automatic grid generator is needed to generate the new mesh using the information obtained from the old mesh. The most robust one which is implemented here uses the advancing front technique [37,50]. An unstructured grid discretization using 3-noded elements with linear shape functions are considered here where the density is assumed as the flow variable in Eq. (4). In this paper, given the minimum/maximum element size, the constant coefficient c_n and the desired error E^{new}, several remeshing steps are performed every predefined time steps of the solution process in order to guarantee a fine mesh at the final step of the analysis. At each remeshing step, in order to obtain the values of the unknown flow variables to be used in the initial time step with the new mesh, these values are interpolated from the previous one.

3. Aerodynamic analysis tool

3.1. Euler solver

In this paper, an Euler based aerodynamic analyzer named PUMI [48] is utilized. Using Eulerian reference frame, and using conservative variables, the equations can be written as

$$\frac{\partial \mathbf{\Phi}}{\partial t}+\frac{\partial \mathbf{F}_k}{\partial x_k}=0 \quad \text{for } k=1,2,3 \quad (7)$$

where $\mathbf{\Phi}$ is the vector of conservative variables and $\mathbf{F}_k$ is the vector of convective flux along the kth direction.

$$\mathbf{\Phi}=\begin{bmatrix}\rho\\ U_1\\ U_2\\ U_3\\ e\end{bmatrix} \quad \mathbf{F}_i=\begin{bmatrix}U_i\\ u_iU_1+p\delta_{i1}\\ u_iU_2+p\delta_{i2}\\ u_iU_3+p\delta_{i3}\\ u_ih\end{bmatrix} \quad (8)$$

where δ_{ij} is the Kronecker delta. The state vector contains the density, momentum ($U_i=\rho u_i$) and total energy (internal plus external) per unit volume of the fluid. Assuming that the fluid behaves like an ideal gas, the expression for the total energy, enthalpy and equation of states are

$$e=\rho\left(c_vT+\frac{u^2}{2}\right) \quad h=e+p=\rho\left(c_pT+\frac{u^2}{2}\right) \quad p=\rho RT \quad R=c_p-c_v \quad (9)$$

After some calculations, the finite element approximation to the equation set (10) is obtained as

$$\int_\Omega N_i\left(N_j\mathbf{\Phi}^j+\frac{\partial \mathbf{F}_k}{\partial x_k}\right)d\Omega=0 \quad \text{for } i=1,\ldots,n_{node} \quad (10)$$

In Eq. (12), there are as many equations as unknowns; therefore the system can be solved for the nodal values of the approximate solution by applying proper boundary conditions. The integrals in Eq. (10) are evaluated using a Gauss quadrature. It is assumed that the fluxes inside the elements can be interpolated from their nodal values to increase the efficiency of the algorithm. This is equivalent to use a Lobato quadrature for the fluxes and it does not affect the final results significantly. It is the form of

$$\mathbf{F}_k=N_j\mathbf{F}_k(x^j)=N_j\mathbf{F}_k^j \quad (11)$$

With this assumption, Eq. (10) can be transformed into Eq. (12)

$$\int_\Omega N_i\left(N_j\mathbf{\Phi}^j+\frac{\partial N_j}{\partial x_k}\left(\mathbf{F}_k^j\right)\right)d\Omega=0 \quad \text{for } i=1,\ldots,n_{node} \quad (12)$$

By defining $\mathbf{M}$ as the consistent finite element mass matrix and $\mathbf{r}$ as the residual vector, the final equation set can be written as Eq. (13)

$$\begin{aligned}\mathbf{\Phi}^j&=\mathbf{M}^{-1}\mathbf{r}\\ \mathbf{M}&=\int_\Omega N_iN_jd\Omega\\ \mathbf{r}&=\int_\Omega N_i\frac{\partial N_j}{\partial x_k}d\Omega\,\mathbf{F}_k^j\end{aligned} \quad (13)$$

For time integration, an explicit multi-stage Runge–Kutta scheme is chosen in order to increase the allowable time step. More information about the current CFD solver can be found in [48].

3.2. Validation of PUMI and adaptive remeshing

In this section one numerical example is presented to validate PUMI software and also to illustrate the performance of the adaptive remeshing method. The mesh generation and mesh refinement are carried out using the pre/post processing system named GiD based on the advancing front technique.

For the validation of CFD analyzer; PUMI, NACA 0012 airfoil is computed at transonic flight conditions of Mach number $M_\infty=0.8$ and an angle of attack $\alpha=1.25°$. PUMI iterates the physical model with predefined time-steps until a predefined density residual is reached (herein 1×10^{-6}). In this example, two meshing strategies have been used as shown in Fig. 2. The first strategy has consisted in using the uniform mesh (6554 nodes and 12,247 elements) shown in Fig. 2(a). The second strategy has consisted in using a AMR procedure starting with an unstructured coarse mesh consisting of 2084 nodes and 3970 elements as shown in Fig. 2(b). Consecutive refinement levels are carried out every 200 time-steps. Fig. 2(c) shows the final adapted mesh consisting of 8721 nodes and 17,245 elements. It can be seen that the adaptive refinements are particularly applied where the shocks occur on the suction and pressure sides of airfoil, and the trailing and leading edges. It is notable that the number of degrees of freedom corresponding to the initial mesh and uniform fine mesh are maintained for each candidate analysis during the analysis.

Fig. 3 compares *Cp* distributions obtained by PUMI coupled to the uniform and the adapted meshes, and the AGARD solution shown in Ref. [51] where it is validated by comparing results with the wind tunnel data. It can be seen that numerical results obtained by both uniform and adapted mesh are in good agreement with AGARD however a better agreement can be found using the adaptive remeshing method.

Fig. 4 compares *Cp* contours around NACA 0012 with the uniform and adapted meshes. Both techniques successfully capture the strong shock wave on the suction side of the airfoil as well as the weak shock on the pressure side of NACA 0012 airfoil. It is noticed that the adaptive remeshing method can capture shock waves not only on the surface of the airfoil but also in all over the domain.

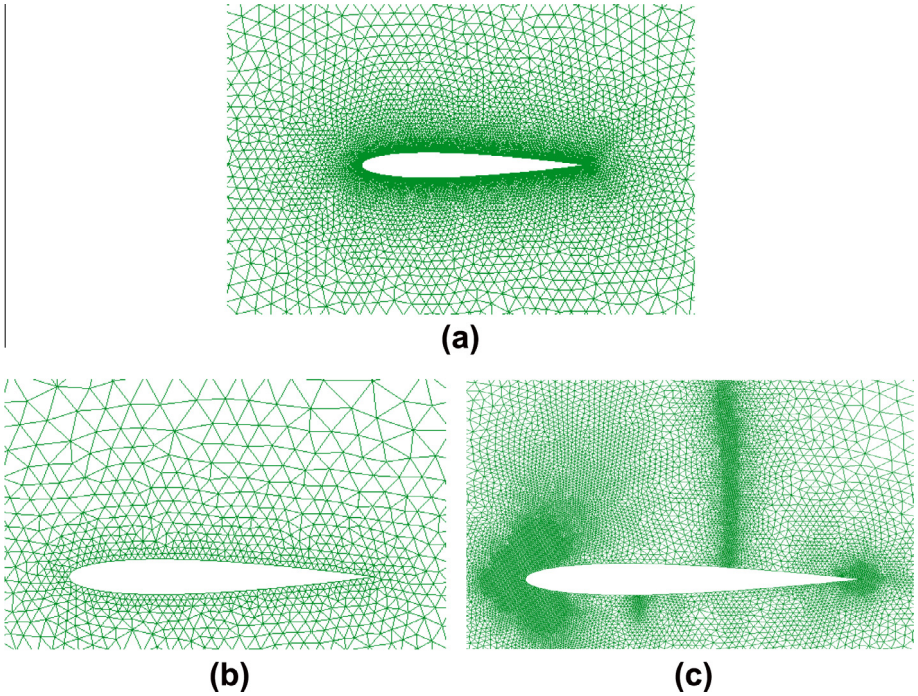

Fig. 2. Mesh conditions around NACA 0012; uniform mesh (a), the adaptive remeshing technique; initial mesh (b), adapted mesh (c).

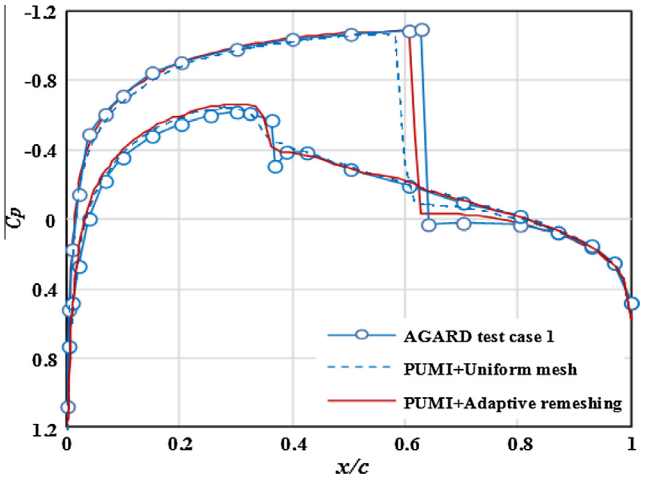

Fig. 3. *Cp* distribution comparison.

4. Aerodynamic design optimization using MOGA coupled to adaptive mesh refinement technique

In this section, two single-objective and one multi-objective design optimizations are conducted using MOGA coupled with both the uniform mesh and the adaptive remeshing approaches. Both methods are validated by solving the first test case and then they are implemented for two more practical test cases. Numerical results obtained by both methods are compared in terms of solution accuracy and computational cost to demonstrate the advantages of adaptive mesh refinement coupled to MOGA.

4.1. Formulation of design problem

For the uniform mesh case, a fine mesh is applied to the analysis of each candidate design whereas a relatively coarse mesh followed by some remeshing steps is implemented for the adaptive mesh refinement. As described in Section 3.3, the number of degrees of freedom corresponding to the uniform mesh is similar

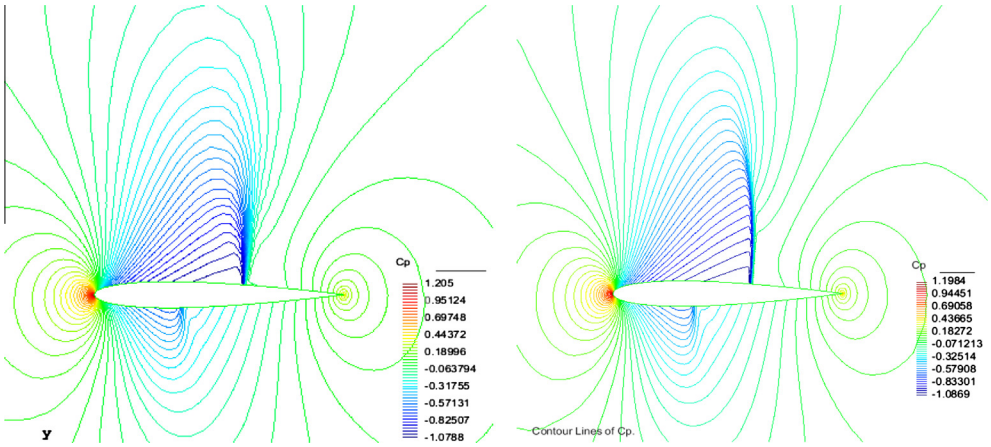

Fig. 4. *Cp* contours of the uniform mesh (left) and adapted mesh (right) around NACA 0012.

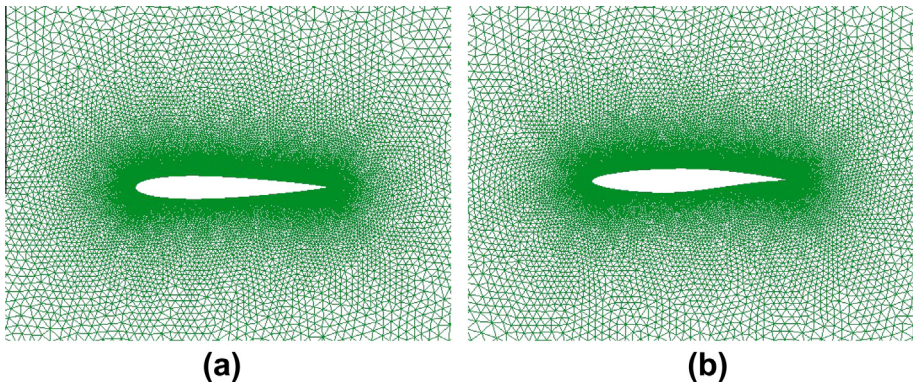

Fig. 5. The baseline mesh around NACA 0012 (a) and RAE 2822 (b).

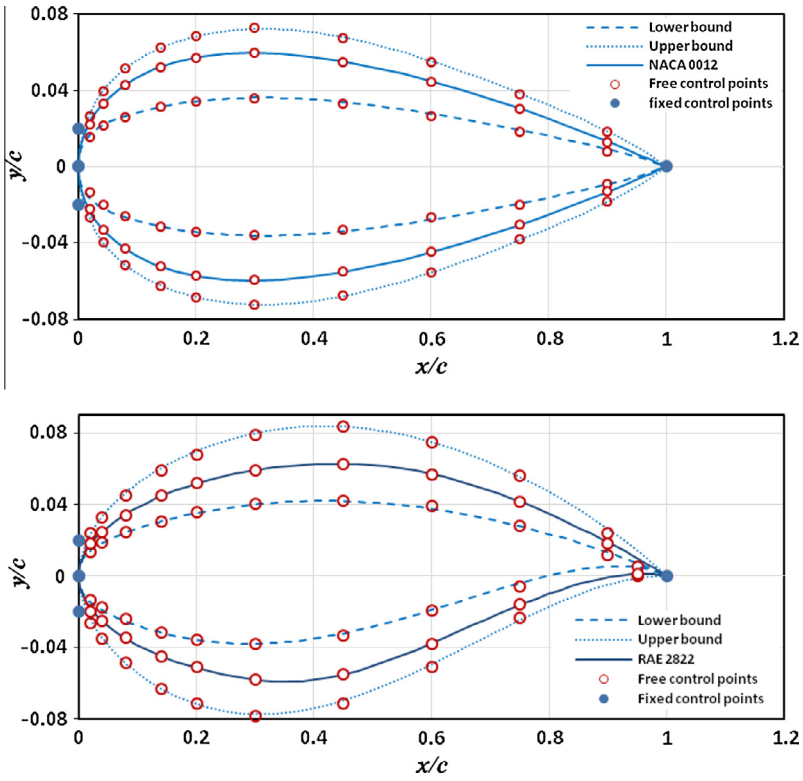

Fig. 6. Upper and lower bound of design variables for NACA 0012 (top) and RAE 2822 (bottom) in comparison with the original ones and corresponding free and fixed control points.

for all candidate designs during each optimization example. As well, this idea is assumed for the number of degrees of freedom corresponding to the coarse mesh. To make a fair comparison of two methods, a fixed number of adaptive remeshing steps is applied to each design candidate to keep a computational cost almost similar to the one for the uniform mesh. It is notable that the additional costs due to the element size calculation and grid regeneration are also taken into account. Hence, the computational time per generation for adaptive remeshing approach will be almost equal to the one of uniform mesh test case.

A fine uniform mesh shown in Fig. 5 is used for the baseline design to compare the final results. A mesh independent study has been carried out in several flight conditions in order to find an appropriate mesh for the baseline design. The minimum element size considered for the baseline mesh is 2.5 times finer than the one implemented for the uniform mesh and for the adaptive remeshing. Indeed, it is dense enough in the vicinity of the airfoil to

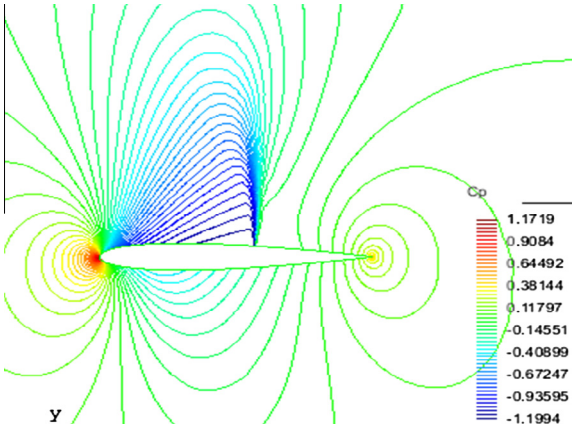

Fig. 7. *Cp* contours around NACA 0012.

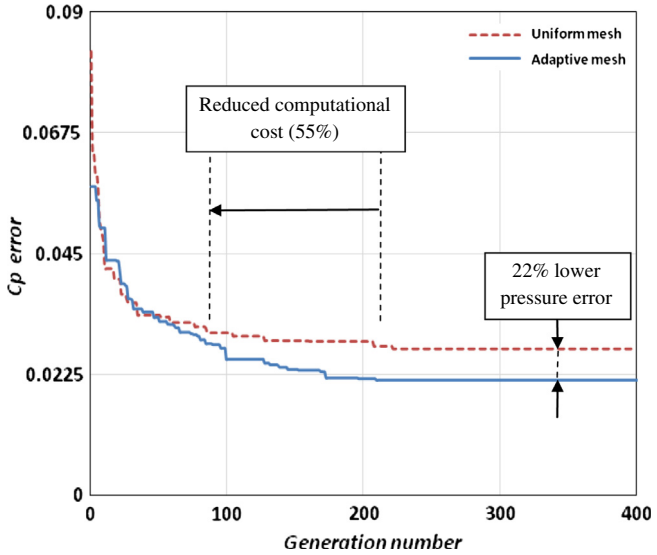

Fig. 8. Convergence history for reconstruction design optimization using MOGA coupled with uniform and adaptive remeshing approaches.

Table 1
Comparison of fitness function values obtained from adaptive remeshing and uniform mesh test cases by eliminating the effect of mesh difference.

Mesh Type	Adaptive remeshing	Uniform mesh
Pressure error	0.0174 (−24%)	0.0230

predict the results in an accurate manner. Fig. 5(a) exhibits the baseline mesh on NACA 0012 consisting of 23,968 nodes and 47,006 elements and that one on RAE 2822 is shown in Fig. 5(b) including 24,017 nodes and 47,091 elements.

4.2. Parameterization for airfoil design

Bezier curves [52] are utilized to represent the geometry of the airfoil as a linear combination of the Bezier polynomial. Given a set of $N+1$ control points, the corresponding Bezier curve is defined as

$$\mathbf{X}(t) = \sum_{i=0}^{N} B_{i,N}(t)\mathbf{R}_i \quad B_{i,N} = \binom{n}{i} t^i (1-t)^{n-i} \tag{14}$$

where $t \in [0, 1]$ denotes the curve parameter, $B_{i,N}(t)$ are the Bezier polynomials of order N and R_i are the coordinates of the control points. The different smooth curves are created by changing these control points.

The geometries of the airfoils used in this work (NACA 0012 and RAE 2822) are represented using 24 control points as shown in Fig. 6. To represent the airfoil geometry accurately, a bigger density of control points is placed close to the zone where the airfoil curve has a bigger curvature. The y coordinates of the control points are considered as the design variables while fixing x coordinates. Two control points, at the leading edge and the trailing edge, have fixed values during the optimization to keep the chord length constant. Also, two other control points near the leading edge are fixed to obtain enough curvature in that zone. In total, 20 design variables are considered for the optimization problems in Sections 4.3, 4.4 and 4.5.

Fig. 6 also shows the upper and lower bounds for the design variables corresponding to both airfoils. This defines a wide range of different geometries which are sufficient for the optimization.

4.3. Reconstruction design optimization of transonic airfoil

4.3.1. Problem definition

This test case considers a single-objective reconstruction design of NACA 0012 using MOGA coupled with the uniform mesh and the adaptive remeshing approaches at flow conditions $M_\infty = 0.78$ and

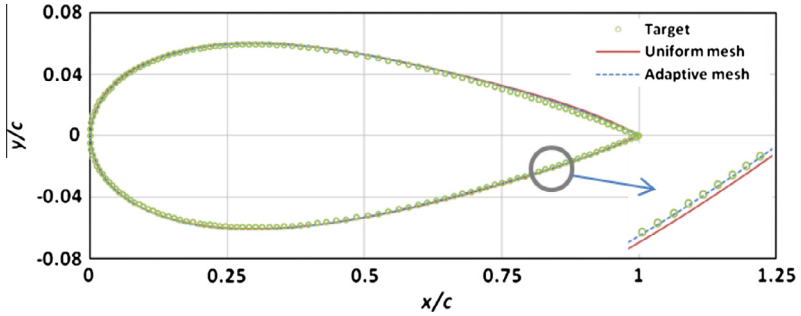

Fig. 9. Comparison geometries obtained by the target and optimal airfoils from the uniform mesh and adaptive remeshing approaches.

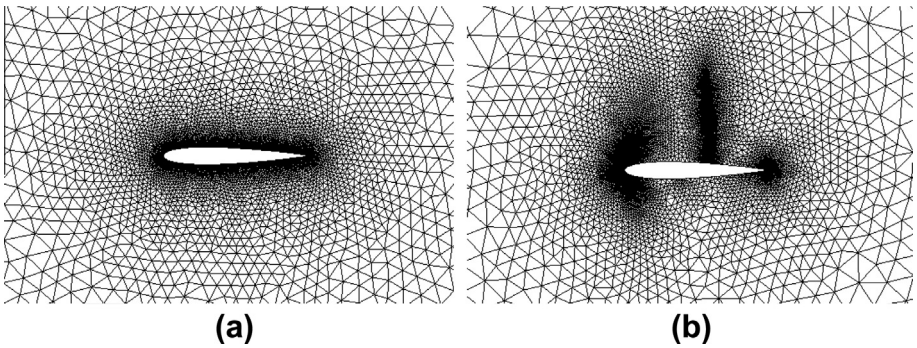

Fig. 10. Mesh conditions around optimal airfoils; uniform mesh test case (a) and adaptive mesh test case (b).

$\alpha = 2.0°$. The main objective is to minimize the pressure error between the target pressure coefficient C_p^* and the candidate one. The fitness function uses the least square error of the pressure shown in Eq. (15)

$$f = \frac{1}{N}\sum_{i=1}^{N}(C_p - C_p^*)^2 \tag{15}$$

where N represents the number of pressure points on the airfoil ($N = 200$). As shown in Section 4.2, the y coordinate of the control points around the airfoil are considered as the design variables.

Fig. 7 shows the target pressure contour obtained using the baseline mesh around NACA 0012 shown in Fig. 5(a).

4.3.2. Interpretation of numerical results

Fig. 8 compares the convergence history for pressure error obtained by MOGA coupled with the uniform mesh and the adaptive remeshing approaches. Both test cases were allowed to run for 133 h and 400 generation using a single 4×2.8 GHz processor. The uniform mesh approach achieves an optimal airfoil with pressure error of 0.0273 after 222 generations (74 h). The adaptive remeshing technique coupled with MOGA converged to the pressure error of 0.0213 after 208 generation. This reflects that the adaptive remeshing technique produces a 22% more optimum solution. In addition, the adaptive remeshing technique captures the converged value of the uniform mesh method after 99 generations (33 h) which is only 45% of uniform mesh computational cost. In other words, the adaptive remeshing method saves 55% of the computational cost of the uniform mesh approach. The main reason that the adaptive remeshing method can produce a more improved solution within low computational cost is that the final adapted mesh conditions provide a better environment to simulate flow phenomena when compared to the uniform mesh approach.

To make a fair comparison of the pressure error, the baseline mesh conditions are constructed on each of the optimal airfoils obtained by both methods. Table 1 compares the value of pressure error obtained by optimal airfoils from the uniform mesh and the adaptive remeshing approaches. It can be seen that the optimal airfoil of the adaptive remeshing method produces 24% lower pressure error when compared to the optimal airfoil of the uniform mesh method.

The geometries of the target airfoil and optimal airfoils obtained by the uniform mesh and the adaptive remeshing approaches are compared in Fig. 9. Even though both approaches can capture the target geometry, the adaptive remeshing technique produces a geometry which has a better agreement to the target airfoil when

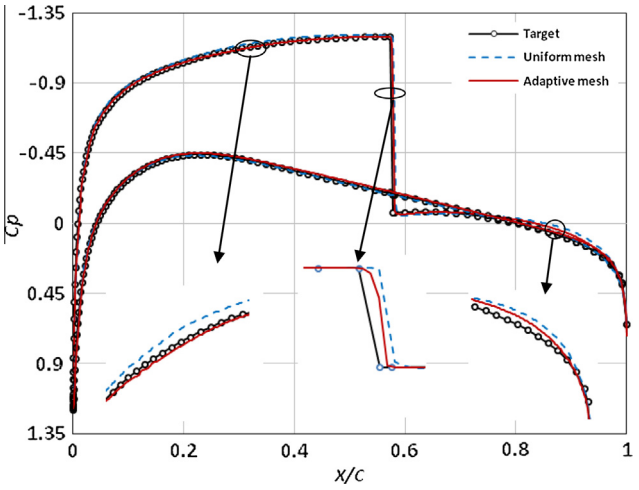

Fig. 11. Comparison of *Cp* distributions obtained by the target, and optimal airfoils from uniform mesh and adaptive remeshing approaches.

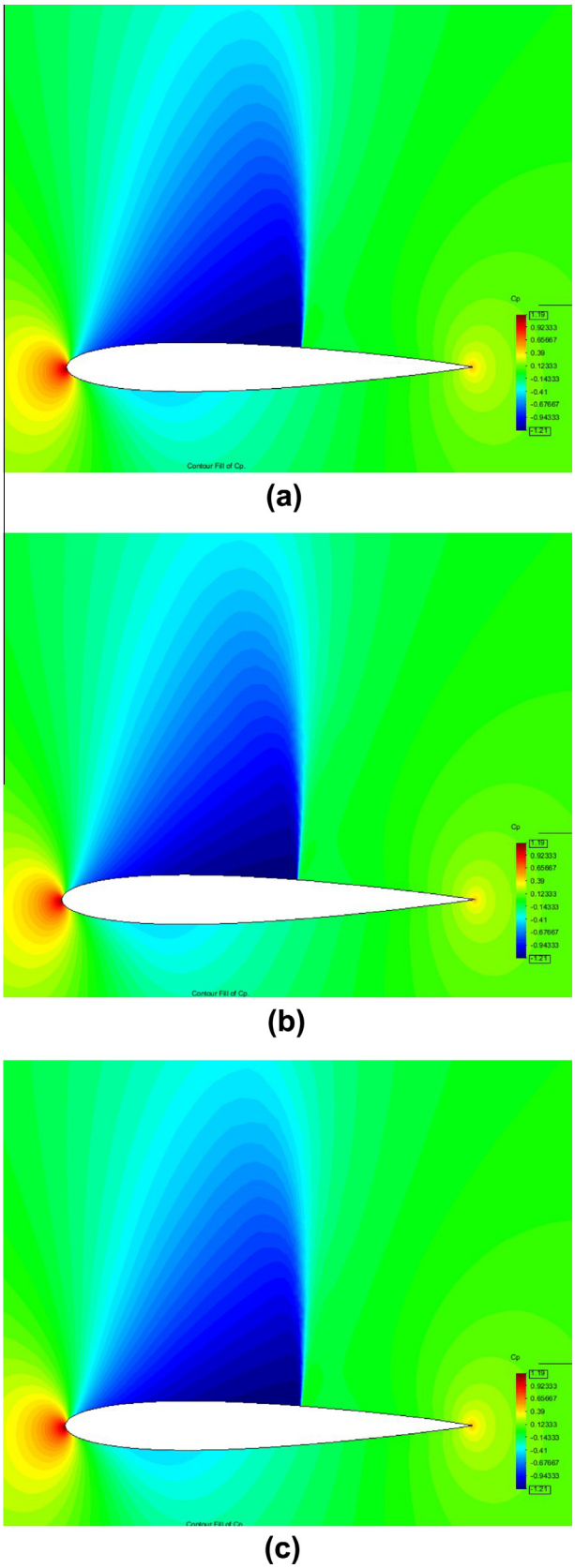

Fig. 12. *Cp* contours around the target airfoil (a), uniform mesh (b) and adaptive remeshing (c) at *Cp* range of [−1.21:1.19].

compared with the optimal airfoil from the uniform mesh approach.

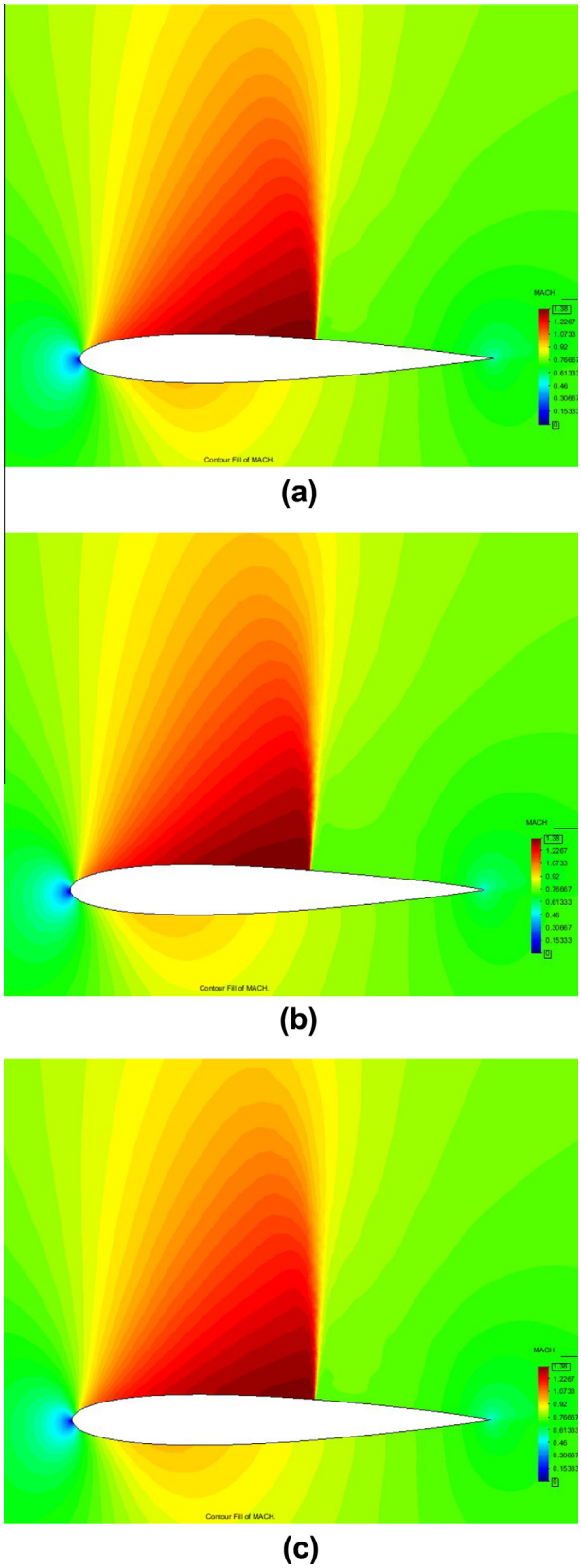

Fig. 13. Mach contours obtained by the target airfoil (a), uniform mesh (b) and adaptive remeshing (c) at Mach range of [0.0:1.38].

Fig. 10(a) shows the generated mesh on the optimized airfoil obtained from uniform mesh test case consisting of 6924 nodes and 13,774 elements whereas that one obtained from adaptive mesh test case is exhibited in Fig. 10(b) including 7161 nodes and 14,139 elements.

Fig. 11 compares *Cp* distributions obtained for the target and both optimal airfoils with the baseline mesh conditions. It can be seen that both optimization approaches made a good agreement to the target pressure distribution on the lower surface of the airfoil while the adaptive remeshing technique produces a closer pressure distribution to the target one on the upper surface.

The corresponding *Cp* contours and Mach contours obtained by the target and both optimal airfoils are illustrated in Figs. 12 and 13 where there are a good agreement in both pressure and Mach. It can also be found that there is a similar contour (minimum and maximum) range to the target one.

4.4. Transonic airfoil design optimization for drag minimization

4.4.1. Problem definition

The test case considers a single-objective design problem for drag minimization of RAE 2822 using MOGA coupled with the uniform mesh and the adaptive remeshing methods at the fixed flow conditions $M_\infty = 0.78$ and $\alpha = 3.0°$. The fitness function is to maximize the lift to drag ratio subjected to a geometry constraint as shown in Eqs. (16) and (17).

$$f = 1/(L/D) \tag{16}$$

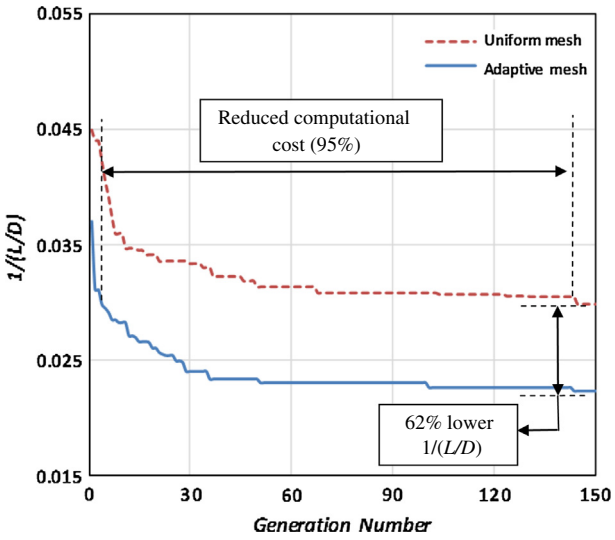

Fig. 14. Convergence history for drag minimization.

Table 2
Comparison of fitness function values obtained from baseline RAE 2822, adaptive remeshing and uniform mesh test cases.

Mesh type	Baseline	Adaptive remeshing	Uniform mesh
$1/(L/D)$	0.04232	0.02221 (−48%)	0.02979 (−30%)

Table 3
Comparison of fitness function values obtained from baseline RAE 2822, adaptive remeshing and uniform mesh test cases by eliminating the effect of mesh difference.

Mesh type	Baseline	Adaptive remeshing	Uniform mesh
$1/(L/D)$	0.0439	0.0205 (−53%)	0.0242 (−45%)

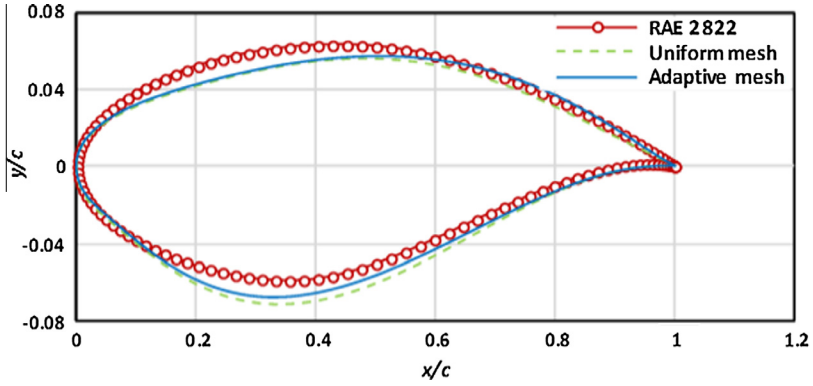

Fig. 15. The comparison between the baseline RAE 2822, the adaptive remeshing and uniform mesh test case.

subject to

$$(t/c)_{\max} \geqslant 0.1211 \tag{17}$$

where L/D and t/c represent the lift to drag ratio and the thickness ratio of the airfoil, respectively. As shown in Section 4.2, the y coordinate of the control points around the airfoil are considered as the design variables.

4.4.2. Interpretation of numerical results

As illustrated in Fig. 14, both MOGA coupled with the uniform mesh and the adaptive remeshing techniques are allowed to run for 150 generations (50 h) using a single 4×2.8 GHz processor. The uniform mesh test case has converged to $f = 0.02979$ after 142 generations (47.3 h). This value is captured by the adaptive remeshing approach after 8 generations (2.67 h). In other words, the adaptive remeshing method improves the optimization efficiency by 95% when compared with the adaptive remeshing technique.

The fitness value resulted from the target design and the optimal design obtained by the uniform and the adaptive methods are compared in Table 2. Both optimal airfoils obtained by the uniform and the adaptive remeshing techniques improve significantly the aerodynamic performance. It can be found that the adaptive method improves the aerodynamic performance by 48% when compared with the baseline design while an improvement of 30% is resulted with the uniform mesh method. Since the shock wave is captured accurately by using AMR technique, the calculated drag and lift coefficients are more reliable. This causes that the adaptive mesh test case provides a better quality solution in less computational cost.

To make a fair comparison, the objective function $(1/(L/D))$ is recomputed by implementing the baseline mesh conditions to both optimal airfoils obtained by the uniform and the adaptive remeshing approaches. The fitness value of the optimal airfoil from the uniform mesh approach is 0.0242. This value is captured by the optimal airfoil of the adaptive remeshing technique with the baseline mesh conditions after 36 generations when the computational cost is only 25% of the uniform mesh method. This shows that the adaptive remeshing technique improves the efficiency of the optimization by 75%.

The objective function corresponding to optimal airfoils obtained by both approaches (using the baseline mesh conditions) are compared in Table 3. It can be seen that the uniform mesh increases the quality of the optimal airfoil by 45% in comparison with the baseline design while an improvement of 53% is resulted by the adaptive remeshing approach. Hence, it can be said that the adaptive remeshing approach improves the aerodynamic behavior a 32.7% compared with the uniform mesh approach.

The geometries of the baseline and both optimal airfoils obtained by the uniform and the adaptive remeshing techniques are compared as shown in Fig. 15. The effect of adaptive remeshing on the optimal airfoil is distinctive in the lower surface as well as the upper surface.

Table 4 compares the airfoil characteristics such as the maximum thickness and the maximum camber for the baseline design and both optimal airfoils from the uniform and the adaptive remeshing techniques. Both optimal airfoils from the uniform and the adaptive remeshing techniques have lower camber while

Table 4
Airfoil configuration of the baseline RAE 2822 and optimized airfoils using adaptive remeshing and uniform mesh.

Mesh type	Baseline	Adaptive remeshing	Uniform mesh
$(t/c)_{\max}$	12.11% (@ 37%)	12.14% (@ 37%)	12.48% (@ 37%)
$camber_{\max}$	1.26% (@ 75%)	1.17% (@ 78%)	1.11% (@ 26%)

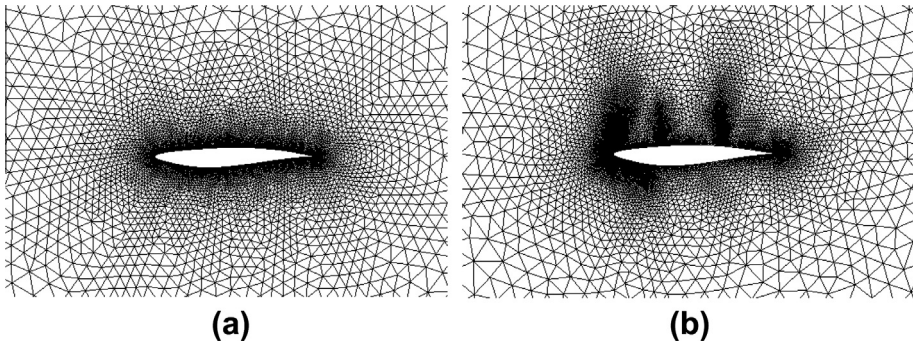

Fig. 16. Mesh conditions around optimal airfoils; uniform mesh test case (a) and adaptive mesh test case (b).

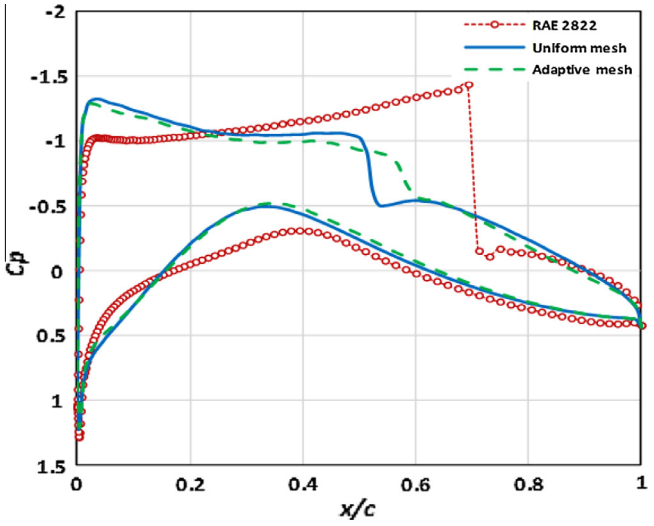

Fig. 17. *Cp* distributions obtained by the baseline design, and optimal airfoils of the uniform mesh and adaptive remeshing.

maintaining similar thickness ratio when compared with the baseline design.

Fig. 16(a) shows the generated mesh on the optimized airfoil obtained from uniform mesh test case consisting of 6946 nodes and 13,749 elements whereas that one obtained from adaptive mesh test case is exhibited in Fig. 16(b) including 7161 nodes and 14,239 elements.

The *Cp* distributions obtained by the baseline design, the uniform mesh and the adaptive remeshing techniques are compared as shown in Fig. 17 using the baseline mesh for each one. It can be seen that both test cases reduce the intensity of the shockwave efficiently while the optimal airfoil obtained by the adaptive remeshing technique has a weaker shockwave when compared to the uniform mesh optimal solution.

Figs. 18 and 19 compare *Cp* and Mach contours obtained by the baseline design and both optimal airfoils obtained by the uniform mesh and the adaptive remeshing approaches. It can be seen that the strong shock wave on the upper surface of the baseline design is getting weaker by optimizing airfoil geometry especially lower camber (mentioned in Table 5). The drag minimization approach has been successful to decrease the strength of the shock wave on the upper surface of the baseline design.

4.5. Multi-objective airfoil design optimization

4.5.1. Problem definition

In this test case, a multi-objective transonic airfoil shape design optimization problem is conducted to improve transonic aerodynamic characteristics of NACA 0012, especially the lift to drag ratio (L/D) and the lift coefficient (Cl). The fitness functions are defined as shown in Eqs. (18) and (19) where L/D and Cl are maximized to extend aircraft range and to improve its maneuverability, respectively. The optimization has two constraints for geometry (thickness ratio: t/c) and aerodynamic performance (Cl_{min}). The geometry constraint is to maintain the fuel tank size of aircraft and the aerodynamic performance constraint is to have a level flight at flight conditions of $M_\infty = 0.75$ and $\alpha = 3.0°$. This example involves minimization of two objective functions

$$f_1 = 1/(L/D) \tag{18}$$

$$f_2 = 1/Cl \tag{19}$$

subject to

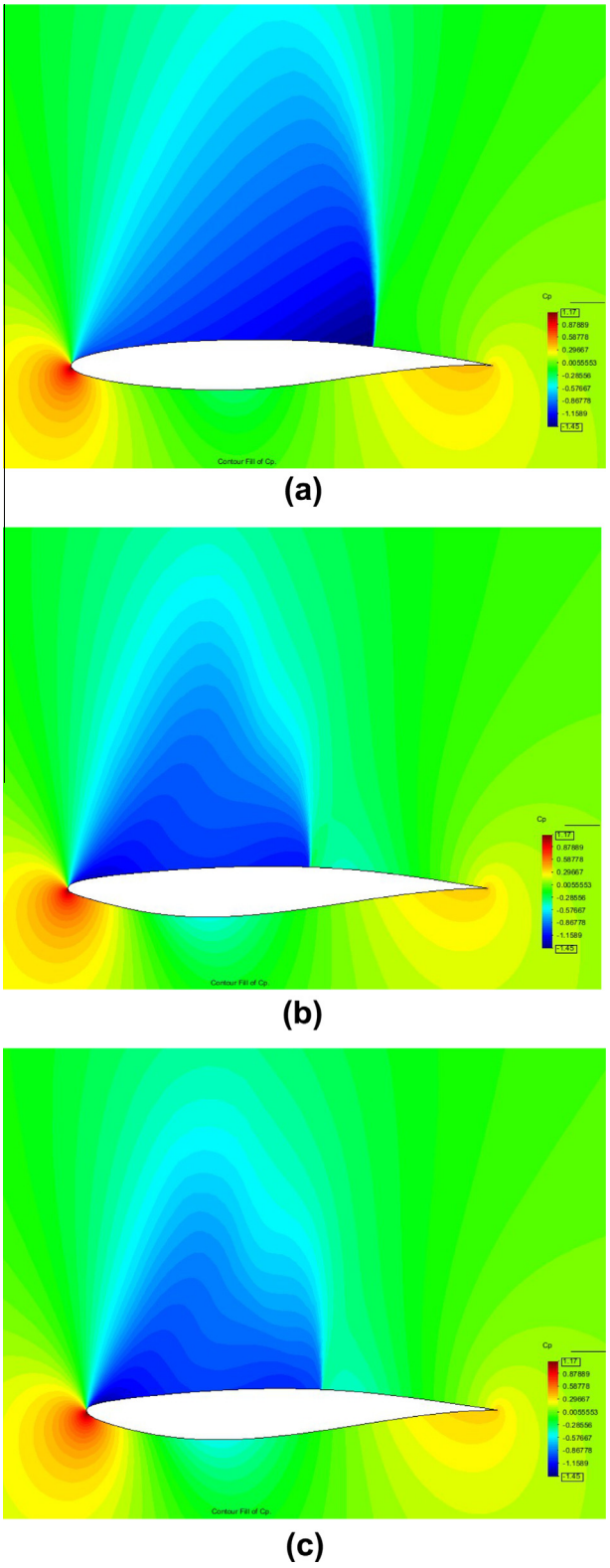

Fig. 18. *Cp* contours around the baseline airfoil (a), uniform mesh (b) and adaptive remeshing (c) at *Cp* range of [−1.45:1.17].

$$t/c_{\max} \geqslant 0.12 \tag{20}$$

$$Cl \geqslant Cl_\infty \tag{21}$$

The lift coefficient constant Cl_∞ is calculated using Eq. (22) which represents the minimum lift coefficient for the aircraft in level flight.

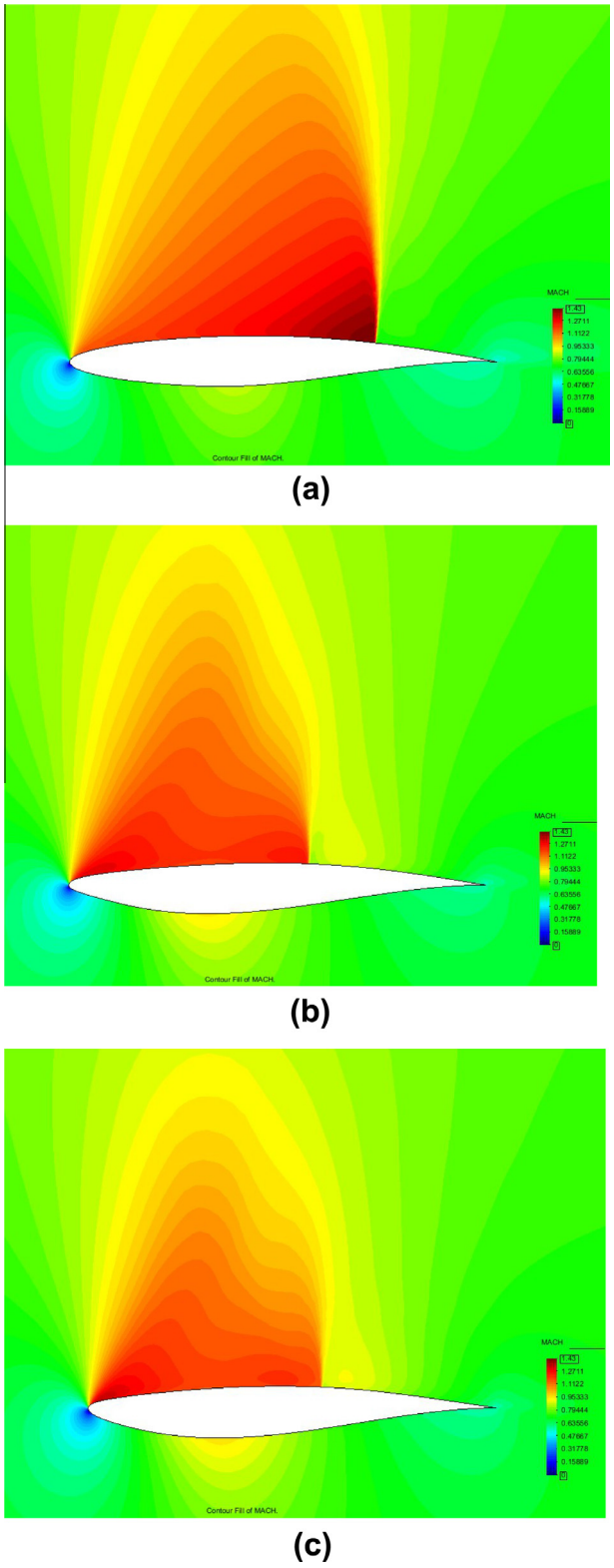

Fig. 19. Mach number contours around the baseline airfoil (a), uniform mesh (b) and adaptive remeshing (c) at Mach range of [0.0:1.43].

$$CL_\infty = 2W/\rho V^2 S \tag{22}$$

where W is the weight force $(m \times g)$ of the aircraft: mass $m = 77{,}564$ kg and acceleration of gravity $g = 9.81$ m/s^2, ρ is the air density at 35,000 *ft*: $\rho = 0.41$ kg/s^3, S is the wing area: $S = 124.58$ m^2, V is the aircraft velocity: $V = 255$ m/s. The Eq. (22) gives $Cl_\infty = 0.45819$. In this case, design parameters for NACA0012 defined in Sectiosn 4.2 are used. Twenty design variables for aerofoil design are considered in total.

Table 5
The comparison of the aerodynamic coefficients for adaptive remeshing approach and the baseline design NACA 0012.

Designs	*Cl*	*Cd*	*L/D*
Baseline	0.5457	0.0279	19.57
Pareto M1	0.5540 (+1.52%)	0.0134 (−51.97%)	41.49 (+112.00%)
Pareto M25	0.6750 (+23.69%)	0.0214 (−23.29%)	31.55 (+61.21%)
Pareto M40	0.7313 (+34.01%)	0.0341 (+22.22%)	21.46 (+9.66%)

4.5.2. Interpretation of numerical results

Two optimization algorithms; MOGA coupled with uniform and adaptive remeshing methods have run 50 h of computer time (150 generations). Fig. 20 compares the baseline design (NACA0012 airfoil) and the Pareto fronts obtained by the uniform mesh and the adaptive remeshing approaches. It can be seen that all Pareto members obtained by both methods dominate the baseline design and the Pareto front obtained by MOGA with the adaptive remeshing technique has a better convergence and divergence when compared to the Pareto front obtained by MOGA coupled with the uniform mesh. Even though the same MOGA is used for both optimizations, the use of adaptive remeshing technique results in speeding up the optimization process while in improving solution accuracy. From the Pareto front obtained by MOGA with adaptive remeshing techniques, the best solutions (Pareto members 1 and 40) for fitness functions 1 and 2, and one of compromised solutions (Pareto member 25) are selected to have further comparisons.

Table 5 compares the aerodynamic characteristics obtained by the baseline design, and by Pareto members 1, 25 and 40. The best solution for the fitness function 1 (Pareto member 1) reduces the total drag (*Cd*) by 51.97% while improving 112% of the lift to drag ratio. The best solution for the fitness function 2 (Pareto member 40) produces 34.01% and 21.46% higher *Cl* and *L/D*. The compromised solution (Pareto member 25) produces 23.69% higher *Cl* and 23.29% lower *Cd* that results in 61.21% *L/D* improvement.

Fig. 21 compares the geometries obtained by the baseline design and Pareto members 1 (the best solution for *f1*), 25 (compromised solution) and 40 (the best solution for *f2*). It can be seen that Pareto optimal solutions 1, 25 and 40 have slightly higher camber

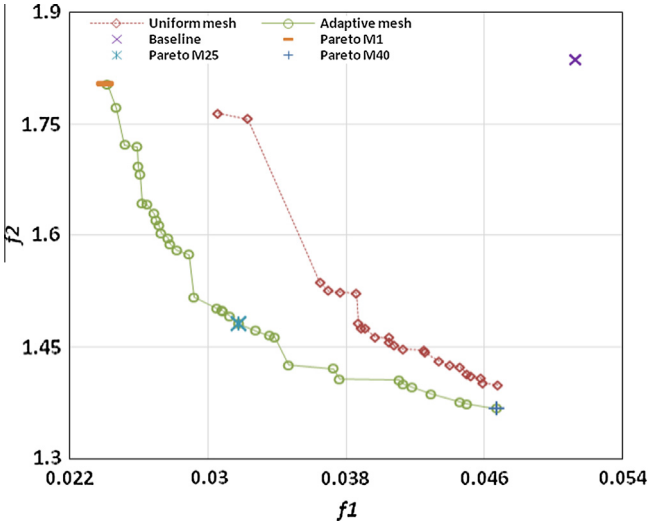

Fig. 20. Optimized Pareto fronts after 150 generations and baseline design.

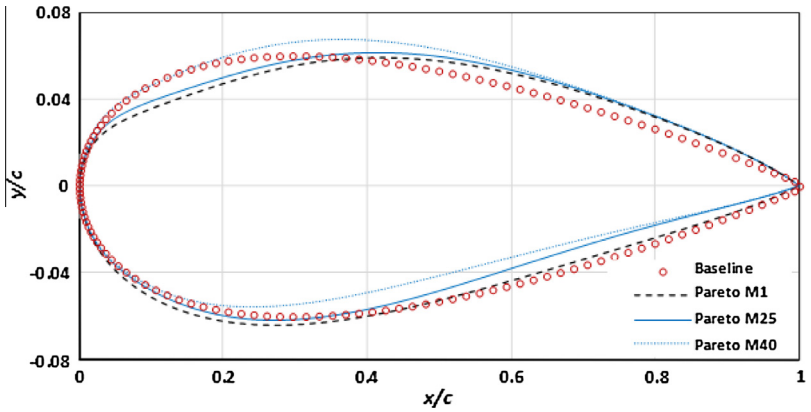

Fig. 21. Geometry comparison between the baseline NACA 0012 and optimal airfoils.

Table 6
Airfoil configuration of the baseline NACA 0012 and the optimized airfoils using adaptive remeshing approach.

	Baseline	Pareto M1	Pareto M25	Pareto M40
$(t/c)_{max}$	12.00% (@30%)	12.03% (@35%)	12.01% (@ 33%)	12.08% (@32%)
$camber_{max}$	0	0.43% (@71%)	0.78% (@67%)	1.11% (@56%)

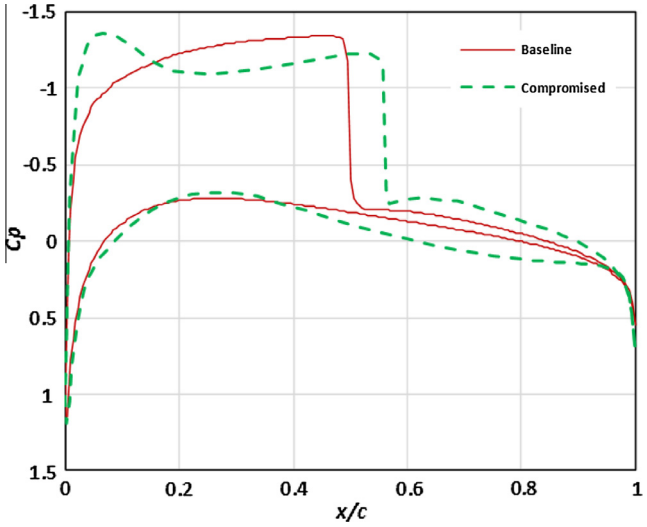

Fig. 22. *Cp* distribution obtained from baseline design and compromised solution.

compared to the baseline design. The geometric characteristics; maximum thickness ration (t/c) and maximum camber, are compared as shown in Table 6. It can be found that there is similarity on the thickness ratio and its position due to the first geometry constraint while the three solutions have different maximum cambers and its positions. The main reason for this difference is that each Pareto member corresponds to a different compromise between the two fitness functions. A separate minimization of each of the fitness functions by solving a single optimization problem would produce two different cambers and positions. Hence, each combination of both fitness functions provided by each Pareto member produces a different solution which is a combination between both single-optimization ones. The obtainment of airfoils with non-zero values for maximum camber is in accordance with this aerodynamics principle of cambered airfoils stating that the increase of the camber improves aerodynamic properties of the airfoil especially the lift coefficient. Indeed, it can be observed in Table 6 that the greatest value for maximum camber is resulted for the Pareto M40 which corresponds to the design giving maximum *Cl* value. Furthermore, Table 6 demonstrates that the least value for maximum camber is obtained for the Pareto M1 which corresponds to the design giving maximum *L*/*D* value with the minimum *Cd* value. This result affirms the behavior seen by transonic and supersonic airfoils that lower camber reduces drag divergence Mach number which consequently decreases the drag coefficient.

Figs. 22 and 23 compares the pressure (*Cp*) distributions and contours obtained by the baseline design and compromised solution (Pareto member 25). It can be seen that the shock position on the suction side of airfoil is moved towards the trailing edge

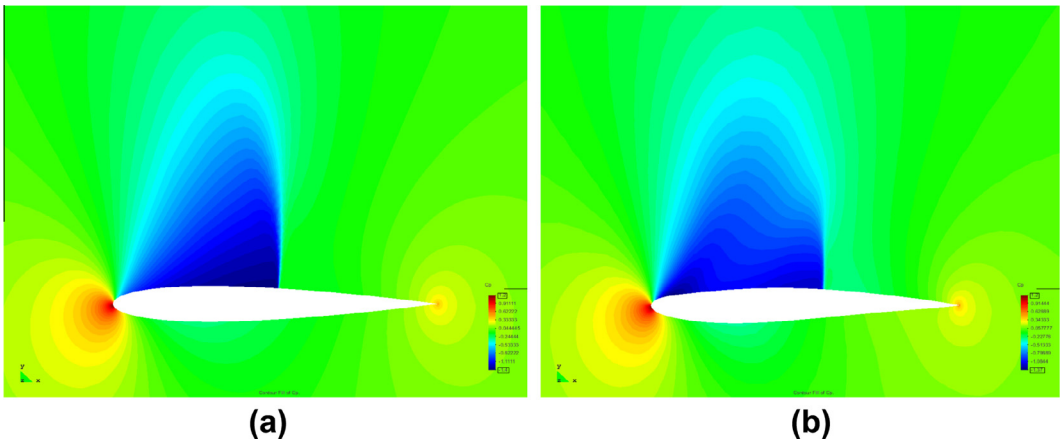

Fig. 23. *Cp* contours obtained by the baseline design (a) and compromised solution (b) at *Cp* range of [−1.37:1.20].

when compared to the baseline design while reducing the strength of shock. It results in improving *Cl* and *L/D* by 23.69% and 61.21% respectively.

5. Conclusion

In this paper, a methodology coupling MOGA and adaptive remeshing approach is developed and it is implemented to three practical aerodynamic shape design optimization problems in a single- and multi-objective manner. From numerical studies, both MOGA coupled to uniform mesh and adaptive remeshing approaches are validated through reconstruction/inverse test case and they are implemented to solve two complex aerodynamic shape design optimizations; drag minimization and multi-objective shape design. It is noticed that despite the same MOGA and CFD analyzer, the use of adaptive remeshing approach accelerates the optimization process while increasing the solution accuracy when compared to the one with uniform mesh technique. Ongoing research focuses on coupling MOGA, Navier–Stokes based CFD analyzer and adaptive remeshing techniques for 3D wing design and implementation of Game theory in adaptive remeshing techniques and its application for robust design optimization are considered for future research avenues.

Acknowledgements

The authors greatly acknowledge Jordi Pons for helpful discussions and suggestions, Enrique Ortega for providing CFD solver and also GiD group in CIMNE.

The second author is grateful for the financial support received for the development of this paper through the research Project DPI2008-05250 of the Ministerio de Ciencia e Innovación (Spain).

References

[1] Sobieszczanski-Sobieski J. The case for aerodynamic sensitivity analysis. In: Presented at the NASA/VPI&SU symposium on sensitivity analysis in engineering; 1986. p. 25-6.
[2] Newman JC, Anderson WK, Whitfield DL. Multidisciplinary sensitivity derivatives using complex variables. MSSU-EIRS-ERC-98-08; 1998.
[3] Pironneau O. On optimal shapes for Stokes flow. J Fluid Mech 1973;70(2):331–40.
[4] Jameson A. Aerodynamic design via control theory. J Sci Comput 1988;3(233):260.
[5] Jameson A, Pierce N, Martinelli L. Optimum aerodynamic design using the Navier–Stokes equations. In: AIAA paper 97–0101, 35th aerospace sciences meeting and exhibit. Reno, Nevada; January 1997.
[6] Reuther J, Jameson A, Alonso JJ, Rimlinger MJ, Saunders D. Constrained multipoint aerodynamic shape optimization using an adjoint formulation and parallel computers. AIAA paper 97–0103.
[7] Anderson WK, Venkatakrishnan V. Aerodynamic design optimization on unstructured grids with a continuous adjoint formulation. Comput Fluids 1999;28(4):443–80.
[8] Castro C, Lozano C, Palacios F, Zuazua E. Systematic continuous adjoint approach to viscous aerodynamic design on unstructured grids. In: AIAA, vol. 45(9). p. 2125.
[9] Elliott J, Peraire J. 3-D aerodynamic optimization on unstructured meshes with viscous effects. In: AIAA paper 97–1849; June 1997.
[10] Mavriplis D. Formulation and multigrid solution of the discrete adjoint for optimization problems on unstructured meshes. In: 43th AIAA aerospace sciences meeting and exhibit. Reno, NV; January 2005.
[11] Anderson MB. Using pareto genetic algorithms for preliminary subsonic wing design. In: AIAA 1996–4023.
[12] Holst TL. Genetic algorithms apply to multi-objective aerodynamic shape, optimization. In: NASA/TM-05-212846; 2005.
[13] Nemec M, Zingg DW, Pulliam TH. Multipoint and multi-objective aerodynamic shape optimization. In: 9th AIAA/ISSMO symposium on multidisciplinary analysis and optimization. AIAA paper 2002-5548. Atlanta; September 2002.
[14] Goldberg DE. Genetic algorithm in search, optimization and machine learning. Massachusetts: Addison-Wesley; 1989.
[15] Deb K, Pratap A, Agrawal S, Meyarivan T. A fast elitist non-dominated sorting genetic algorithm for multi-objective optimization: NSGA-II. IEEE Trans Evol Comput 2002;6(2):182–97.
[16] Gage P, Kroo I. A role for genetic algorithm un a preliminary design environment. In: AIAA 93-3933, AIAA aircraft design, systems and operations meeting. Monterey, CA; August 1993.
[17] Crispin Y. Aircraft conceptual optimization using simulated. Evolution; AIAA-94-0092; 1994.
[18] Quagliarella D, Cioppa AD. Genetic algorithms applied to the aerodynamic design of transonic airfoils. AIAA-94-1896-CP; 1994.
[19] Crossley AW, Laananen HD. Conceptual design of helicopters via genetic algorithm. J Aircraft 1996;3(6) [November–December].
[20] Periaux J, Mantel B, Sefrioui M, StouUet B, Desideri JA, Lanteri S, et al. Evolutionary computational methods for complex design in aerodynamics. AIAA-98-0222, Reno; 1998.
[21] Wang JF, Periaux J, Sefriouib M. Parallel evolutionary algorithms for optimization problems in aerospace engineering. J Comput Appl Math 2002;149(1):155–69.
[22] Quagliarella D, Vicini A. Viscous single and multicomponent airfoil design with genetic algorithms. Finite Elem Anal Des 2001;37(5):365–80.
[23] Periaux J, Lee DS, Gonzalez LF, Srinivas K. Fast reconstruction of aerodynamic shapes using evolutionary algorithms and virtual Nash strategies in a CFD design environment. J Comput Appl Math 2008;232(1):61–71.
[24] Yamamoto K, Inoue O. Applications of genetic algorithm to aerodynamic shape, optimization. AIAA-95-1650-CP; 1995.
[25] Obayashi S. Pareto genetic algorithm for aerodynamic design using the Navier–Stokes equations. Genetic Algorithms Eng Comput Sci 1998:245–66.
[26] Obayashi S. Pareto solutions of multipoint design of supersonic wings using evolutionary algorithms. In: Proc 5th int conf on adaptive computing in design and manufacture. Exeter, Devon, UK; April 2002.
[27] Obayashi S, Nakahashi K, Oyama A, Yoshino N. Design optimization of supersonic wings using evolutionary algorithms. In: Proc ECCOMAS 98. John Wiley & Sons; 1998.
[28] Pulliam TH, Nemec M, Holst T, Zingg DW. Comparison of evolutionary (genetic) algorithm and adjoint methods for multi-objective viscous airfoil optimizations. AIAA-03-0298; 2003.
[29] Oyama A, Obayashi S, Nakahashi K. Transonic wing optimization using genetic algorithm. In: 13th Computational fluid dynamics conference. AIAA paper 97–1854; June 1997.
[30] Kroo I, Altus S, Braun R, Gage P, Sobieski I. Multidisciplinary optimization methods for aircraft preliminary design. In: AIAA/NASA/USAF/ISSMO symposium on multidisciplinary analysis and optimization. AIAA 94-4325. Panama City, FL; September 7–9, 1994.
[31] Makino Y, Aoyama T, Iwamiya T. Numerical optimization of fuselage geometry to modify sonic-boom signature. J Aircraft 1999;36(4):668–74.
[32] Alonso JJ, Kroo IM, Jameson A. Advanced algorithms for design and optimization of quiet supersonic platform. In: 40th AIAA aerospace sciences meeting & exhibit. AIAA paper 2002-0144, Reno, NV; January 2002.
[33] Quagliarella D, Chinnici G. Usage of approximation techniques in evolutionary algorithms with application examples to aerodynamic shape design problems. In: Annicchiarico W, Periaux J, Cerrolaza M, Winter G. editors. Evolutionary algorithms and intelligent tools in engineering optimization. CIMNE; 2005. p. 167–89.
[34] Vicini A, Quagliarella D. Airfoil and wing design through hybrid optimization strategies. AIAA J 1999;37(5):634–41.
[35] Chung H, Choi S, Alonso J. Supersonic business jet design using knowledge-based genetic algorithm with adaptive, unstructured grid methodology. In: 21st AIAA applied aerodynamics conference. AIAA paper 2003-3791. Orlando, FL; June 23–26, 2003.
[36] Zienkiewicz OC, Wu J. Automatic directional refinement in adaptive analysis of compressible flows. Int J Numer Meth Eng 1994;37:2189–210.
[37] Peraire J, Vahdati M, Morgan K, Zienkiewicz OC. Adaptive remeshing for compressible flow computations. J Comput Phys 1987;72:449–66.
[38] Nithiarasu P, Zienkiewicz OC. Adaptive mesh generation for fluid mechanics problems. Int J Numer Meth Eng 2000;47:629–62.
[39] Palmerio B, Dervieux A. Application of a FEM moving node adaptive method to accurate shock capturing. In: Proceeding of first international conference on numerical grid generation in CFD. Landshut, W. Germany; 1986.
[40] Jacquotte OP, Cabello J. Three-dimensional grid generation method based on a variational principle. La Recherche Aerospatiale 1990;4:8–19.
[41] Löhner R. An adaptive finite element scheme for transient problems in CFD. Comput Methods Appl Mech Eng 1987;61:323–38.
[42] Mavriplis C. A posteriori error estimators for adaptive spectral element techniques. In: Proc 8th GAMM conf num meth fluid mech. NNFM, vol. 29. pp. 333–42, Vieweg.
[43] Löhner R. Adaptive remeshing for transient problems. Comput Methods Appl Mech Eng 1989;75:195–214.
[44] Bugeda G, Oñate E. Optimum aerodynamic shape design including mesh adaptivity. Int J Numer Methods Fluid 1995;20:915–34.
[45] Bugeda G, Oñate E. Optimum aerodynamic shape design for fluid flow problems including mesh adaptivity. Int J Numer Methods Fluid 1998;30:161–78.
[46] Lee DS, Bugeda G, Periaux J, Onate E. Robust active shock control bump design optimization using parallel hybrid-MOGA. In: The 23rd international conference on parallel computational fluid dynamics, vol. 211. Barcelona, Spain; 16–20 May, 2011.
[47] Lee DS, Periaux J, Onate E, Gonzalez LF. Advanced computational intelligence system for inverse aeronautical design optimization, International Conference on Advanced Software Engineering (ICASE-11). In: Proceedings of the 9th IEEE

international symposium on parallel and distributed processing with applications workshops, ISPAW 2011 - ICASE 2011, SGH 2011, GSDP 2011, ISBN (978-1-4577-0524-3), Busan, Korea; 26–28 May, 2011. p. 299–304.
[48] Flores R, Ortega E, Oñate E. PUMI: an explicit 3D unstructured finite element solver for the Euler equations. Publication CIMNE; 2008; PI 326.
[49] Löhner R. Mesh adaptation in fluid mechanics. Eng Fract Mech 1995;50(5/6):819–47.
[50] Löhner R. Some useful data structures for the generation of unstructured grids. Comm Appl Num Meth 1988;4:123–35.
[51] Pulliam TH, Barton JT. Euler computations of AGARD Working Group 07 Airfoil Test Cases. In: AIAA 23rd aerospace summer meeting. AIAA Paper, Reno, NE; 1985; 85–0018.
[52] Faux ID, Pratt MJ. Computational geometry for design and manufacture. Ellis Horwood Limited; 1987.